NUMERICAL STUDY ON MODE TRANSITION OF AN OPEN CAVITY WITH LIDS

Dae Nyoung HEO † **Jae Wook KIM** ‡ **Duck Joo LEE** ♯

Abstract

When fluid flows at a certain speed over an open cavity, large pressure fluctuation is produced. This fluctuation acts as an acoustic source and induces the damage of the stored instrumentation or the structure. The physical phenomena of rectangular open cavities with lids are numerically investigated in this paper. Two-dimensional compressible Navier-Stokes equations are computed with high-order and high-resolution numerical schemes. The characteristics of cavity resonance and acoustic propagation are analyzed according to the geometric variation of lids existing on the edges of the cavity. The lids change the resonance frequency, sound pressure level, and directivity of acoustic propagation. This also induces the transition of cavity resonance mode. Cross-correlation analysis and the integral form of Rossiter's equation are used to analyze the transition of Rossiter's mode and explain the sudden change of resonance frequency. The present results provide further understanding of cavity resonance and the effects of lids geometry.

Key Words: Cavity Noise, Lid Geometry, Helmholtz Resonator, Navier-Stokes Equation, Computational Aeroacoustis (CAA), High-Order and High-Resolution Schemes

1 INTRODUCTION

When fluid flows at a certain speed over an open cavity, large pressure fluctuation is produced by the impinging of a free shear layer on the downstream edge of the cavity. Cavity noise is induced by this fluctuation. The point of impingement becomes a source of acoustic energy, which propagates to the front wall of the cavity and interacts with the free shear layer. If the frequency and the phase of the acoustic energy coincide with the instabilities of the shear layer, resonance can occur. The energy entering the shear layer at the leading edge is amplified as it is transported to the downstream edge where it interacts. Through these steps, one cycle of a feedback loop is completed. In the case of a vehicle, very loud and uncomfortable noise is generated at an opened sunroof and windows when a vehicle runs at a certain speed. In the case of an airplane, noise is created at the landing gear wells during take-off and landing, and at weapon bays during fighting. These noise sources can lead to high-pressure fluctuations near the walls, which may damage stored instrumentation or the structure itself.

Aeroacoustic characteristics in an open cavity have been studied extensively.[1-7] Original Schlieren photographs of an open cavity were obtained by Krishnamurty.[2] The first description of this feedback process is credited to Rossiter[3], who developed a semi-empirical formula to predict measured resonant frequencies. Tam[4] developed a linear mathematical model to predict the frequencies. Recent experiments conducted by Cattafesta[5] have underscored the complicated nonlinear interaction of different modes, and the possibility of mode switching. Colonius[6][7] have investigated the flow over a rectangular cavity for a range of Mach numbers, cavity aspect ratios, upstream boundary layer thicknesses, and Reynolds numbers. Shieh[8] compared two- and three-dimensional turbulent cavity flows by numerical simulation.

Despite this body of research, most studies have only focused on simple rectangular cavities, while the

Received on October 21, 2003.

† Ph.D Candidate; KAIST
E-mail : nyoung@kaist.ac.kr
‡ Post-Doctoral Fellow; KAIST
E-mail : jwkim@acoustic.kaist.ac.kr
♯ Professor; Division of Aerospace Engineering, Department of Mechanical Engineering, Korea Advanced Institute of Science and Technology; Taejon 305-701, Korea
E-mail : djlee@kaist.ac.kr

general cavity is rectangular with lids at each edge like a Helmholtz resonator. Aircraft landing gear wells, weapon bays, and automobile sunroofs have this shape. As such, the aim of this study is to analyze the physical phenomena of rectangular open cavities with lids. The characteristics of cavity resonance and acoustic propagation are analyzed according to the geometric variation of lids existing on the edges of the cavity. The sudden change of resonance frequency can be explained by the transition of Rossiter's mode.

First, the flow and acoustic fields are numerically simulated. In order to analyze the strongly coupled feedback interaction between flow and acoustics, nonlinear unsteady compressible Navier-Stokes equations are solved by high-order and high-resolution schemes. In order to analyze the transition of Rossiter's mode, cross-correlation analysis and the integral form of Rossiter's equation are used. The cross-correlation shows the characteristics of wave propagation in space and time, and the cross-spectral density, which is defined as the Fourier transform of the cross-correlation function, shows the variation of amplitude ratios and phase angles as a function of frequency. The integral form of Rossiter's equation is designed to develop the accuracy of the original Rossiter's equation by introducing two parameters, effective length and new phase lag, and can predict resonance frequency precisely in various conditions.

2 GOVERNING EQUATIONS AND NUMERICAL METHODS

The governing equations are unsteady compressible Navier-Stokes equations. The flux vector form of the governing equations may be expressed as

$$\frac{\partial Q}{\partial t} + \frac{\partial E}{\partial x} + \frac{\partial F}{\partial y} = S_v \tag{1}$$

where Q is the vectors of the conservative variables, E and F are the Euler fluxes, and is a source term that consists of the viscous flux derivatives. All the components of Q, E, F, and have been fully described in numerous papers[9][10] and textbooks.

High-order and high-resolution numerical schemes are applied to the present computation in a structured grid system to analyze the strongly coupled feedback interactions between the flow and the acoustics. The optimized fourth-order penta-diagonal (OFOP) compact finite difference scheme[9][10] is used for evaluating the flux derivatives. OFOP is an explicit scheme optimized for achieving maximum resolution characteristics. Combined with high-order finite difference schemes in space, the low dissipation and dispersion Runge-Kutta[11] scheme is used for integrating the governing equations in time. The adaptive nonlinear artificial dissipation model[12] is also used to remove unwanted numerical oscillations and implemented only at the last (fourth or sixth) stage of the Runge-Kutta marching in order to minimize computational costs. Characteristic boundary conditions[13] are used for accurate and robust calculation. Nonreflecting inflow/outflow and no-slip wall conditions are imposed effectively at the boundaries. Moreover, the buffer zone technique[14] is employed in a region near inflow/outflow computational boundaries.

In reference 15, the benchmark problem of category 6 in the third computational aeroacoustics (CAA) workshop[16] is studied to validate the accuracy of the numerical methods used in this study. The problem given is to calculate the frequencies and the sound pressure level in dB at the center of the left wall associated with the flow of air over a door gap cavity that is the shape of rectangular cavity having a lid at the leading edge. Reference 15 shows that the predicted SPL spectrum is in good agreement with the experiment in the overall frequency range. The results demonstrate that the numerical methods used in this paper can simulate the flow-acoustics resonance phenomena of a cavity with lids and accurately predict the resonance frequency and the sound pressure level.

3 EFFECTS OF LID GEOMETRY

The flow and acoustic fields of a cavity are studied according to the variation of lid geometry in this section. Schematic diagrams of the cavity configuration and computational domain are shown in figure 1. The upstream laminar Blasius boundary layer is specified along the inflow boundary, and it is characterized by the momentum thickness (θ) of the boundary layer at the cavity leading edge. The Reynolds number ($Re_\theta = U_\infty \theta/\nu$) is based on the free-stream velocity (U_∞), the momentum thickness (θ), and the kinematic viscosity in the ambient flow (ν). The free-stream Mach number is M_∞. The cavity geometry is specified by momentum thickness relative to cavity depth (θ/D), and cavity length relative to depth (L/D) which is called the aspect ratio of the cavity. Lid geometries are specified by their length (W_1, W_2) and thickness (H). Opening length (O) is defined as $O = L - W_1 - W_2$. The length variables of the lid are non-dimensionalized to W_1/D, W_2/D, H/D, and O/D.

In this study, the upstream velocity profile and the

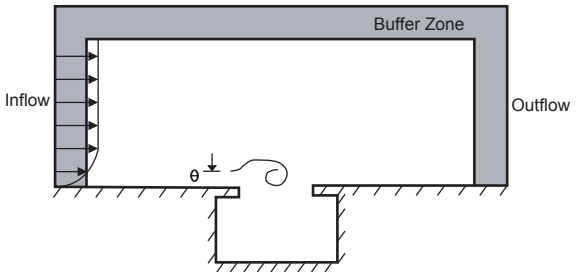

(a) Full computational domain

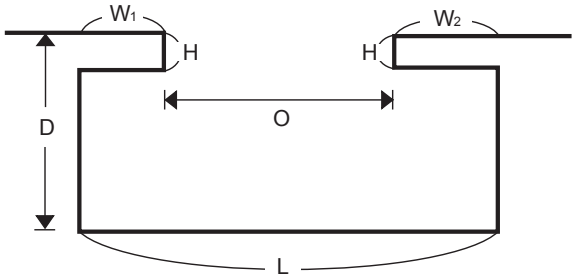

(b) Configuration of cavity geometry

Fig.1: Schematic diagrams of the cavity configuration and computational domain

Case	H/D	W_1/D	W_2/D	O/D	$St = fL/U_\infty$
W0	0	0	0	2	0.66
W1	0.05	0.125	0.125	1.75	0.63
W2	0.05	0.25	0.25	1.5	0.59
W3	0.05	0.375	0.375	1.25	0.59
W4	0.05	0.5	0.5	1	0.53
W5	0.05	0.625	0.625	0.75	0.41
W6	0.05	0.75	0.75	0.5	-
H1	0.05	0.5	0.5	1	0.53
H2	0.1	0.5	0.5	1	0.53
H3	0.15	0.5	0.5	1	0.53
H4	0.2	0.5	0.5	1	0.52
H5	0.25	0.5	0.5	1	0.30
H6	0.3	0.5	0.5	1	0.30
P1	0.2	0	1	1	0.28
P2	0.2	0.25	0.75	1	0.30
P3	0.2	0.5	0.5	1	0.52
P4	0.2	0.75	0.25	1	0.30
P5	0.2	1	0	1	-

Table 1. Dimensions of lid parameters and resultant Strouhal number for each case

aspect ratio of the cavity are the same for all simulations, and the simulation conditions are $M_\infty = 0.5$, $L/D = 2$, $\theta/D = 0.04$, and $Re_\theta = 200$. Under the given conditions, a simple rectangular cavity without a lid shows a typical shear layer mode.[15][17] Three series of cavity geometries are numerically simulated. The first is cavities having twin lids ($W_1/D = W_2/D$) of same thickness ($H/D = 0.05$) and different length. The second is cavities having twin lids ($W_1/D = W_2/D$) of different thickness and same length ($W_1/D = W_2/D = 0.5$). The third is cavities having the same opening length ($O/D = 1$) and different opening position. Through these simulations, the effects of lid length, lid thickness, and opening position are analyzed.

3.1 Effects of Lid Length

The effects of lid length are studied in this section. The cavities have twin lids on each edge, which means the two lids have the same thickness (H/D) and length ($W_1/D = W_2/D$). The lid thickness is constant at $H/D = 0.05$ for all cases, and the lid length varies from $W_1/D = W_2/D = 0$ to $W_1/D = W_2/D = 0.75$. The geometric parameters of each case are shown from case W0 to case W6 in table 1. Case W0 has no lid, and case W6 have the longest lids. The Strouhal number (St) achieved from the far-field acoustic signal is also shown in table 1. The most important feature of these cases is that the Strouhal number (St) becomes smaller as the lid length becomes longer. For W6, steady mode occurs.

Figure 2 shows the instantaneous vorticity ($\omega = \partial v/\partial x - \partial u/\partial y$) contours of case W0 and W4. 20 levels contours are drawn between the non-dimensional vorticity ($\omega D/U_\infty$), -7 and 3. Case W0 shows the typical shear layer mode of a rectangular cavity having no lids. [15][17] Vortices generated from the leading edge convect downstream in the shear layer and impinge on the downstream edge. This impingement induces large pressure fluctuation, which becomes the major acoustic source. Some part of the collapsed vortex enters the inside of cavity and forms a rotating flow which interacts with the vortices in the shear layer. Although case W4 also shows shear layer mode, the vortex strength and the interaction between the vortex in the shear layer and the vortex inside the cavity are relatively weak compared to those of case W0. Because the opening length is short, the vortex in the shear layer cannot develop to be as strong as that of case W0 before collapse. Therefore case W4 induces weaker pressure fluctuation than case W0 and this cavity is relatively quiescent.

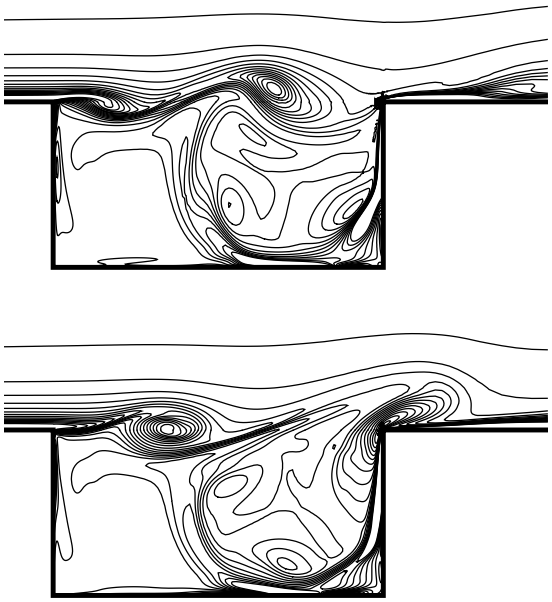

(a) Case W0

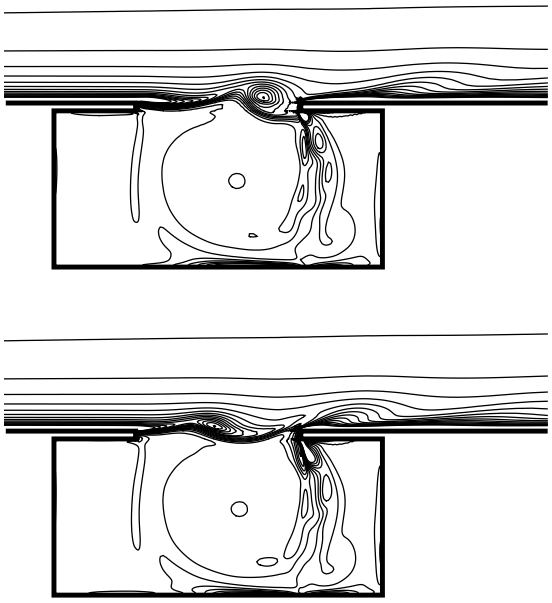

(b) Case W4

Fig.2: Vorticity contours at two instants (20 levels between non-dimensional vorticity, $\omega D/U_\infty = -7$ and 3)

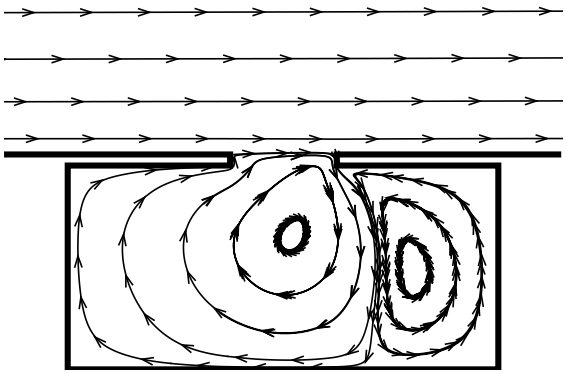

Fig.3: Streamlines of case W6

The streamlines of case W6 are shown in figure 3. No vortex is generated in the shear layer because the length of the cavity opening is too short. A weak vortex occupying the left inner half of the cavity is induced by the velocity of the shear layer at the opening of the cavity, which re-induces another vortex occupying the right half of the cavity. Flow around this cavity maintains a perfectly steady state and no sound is generated from this cavity.

3.2 Effects of Lid Thickness

The effects of lid thickness are studied in this session. Cavities have twin lids on each edge of the cavity ($W_1/D = W_2/D$). The lid thickness varies from $H/D = 0.05$ to $H/D = 0.3$, and the lid length is the same, $W_1/D = W_2/D = 0.5$, for all cases. The geometric parameters are shown from case H1 to case H6 in table 1. The Strouhal number (St) achieved from the far-field acoustic signal is also shown in table 1. The most important feature is that there is a large difference in the Strouhal number between the two groups. The first group is H1, H2, H3, H4, and the second group is H5, H6. Although the Strouhal number of the first group is about 0.53, that of the second group is 0.30. It is anticipated that there is a mode transition between H4 and H5, and this is discussed in detail in the section dealing with mode transition.

In figure 4, the acoustic fields are compared between case W0 and case H4 in order to identify the lid effects on acoustic generation and propagation. Figure 4 shows instantaneous views of the acoustic field over the entire domain except the buffer zones. Dark contours represent expansion and light contours represent compressions. The acoustic waves generated from the cavity are radiated well to far-fields without dissipation. In figure 4(a), the vortex impingement on

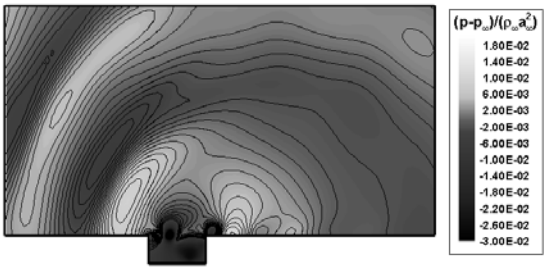

(a) Case W0

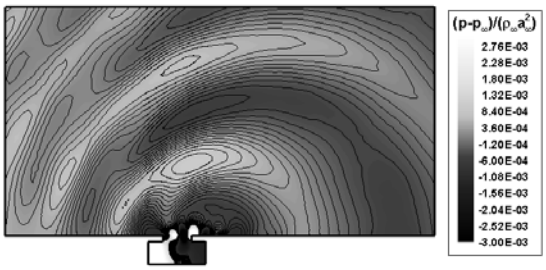

(b) Case H4

Fig.4: Acoustic fields of entire domain except the buffer zones

the downstream edge becomes the dominant acoustic source, and the acoustic waves generated from this propagate to the forward-upper direction. The acoustic wave propagating to the upstream direction has a higher wave number than the wave to the downstream direction because of the free-stream velocity ($M_\infty = 0.5$). In figure 4(b), there are two dominant acoustic sources. The first is the same as that of figure 4(a). The downstream edge, the vortex impingement point, becomes the acoustic source and acoustic waves propagate to the forward-upper direction. The second is the up and down oscillation at the opening. The shape of case H4 is similar to a Helmholtz resonator and the existence of lids induces additional up and down oscillation at the opening. Therefore, this oscillation becomes the second acoustic source and acoustic waves propagate in the upper direction.

3.3 Effects of Opening Position

The effects of opening position are studied in this section. Cavities have different lid length on the each edge of the cavity ($W_1/D \neq W_2/D$). Cases P1, P3 and P5 are forward opening, central opening, and backward opening, respectively. The lid thickness and opening length are the same for all cases, at $H/D = 0.2$ and $O/D = (L - W_1 - W_2)/D = 1$. The geometric parameters of each case are shown from case P1 to case P5 in table 1. The Strouhal number (St) achieved from the far-field acoustic signal is also provided in table 1. The most important feature is that there is a large difference in the Strouhal number (St) between case P3 and the others. Although the Strouhal number of cases P1, P2 and P4 are about 0.30, that of case P3 is 0.52. It is anticipated that there are mode transitions between cases P2 and P3, and between cases P3 and P4. These are discussed in detail in the section concerning mode transition. Another feature that should be noted is that steady mode occurs in case P5.

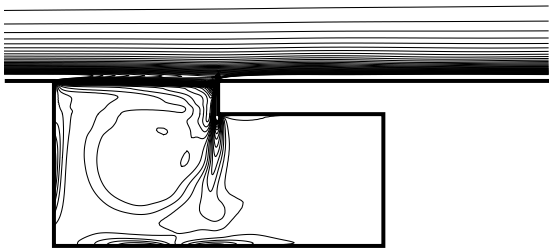

(a) Case P1

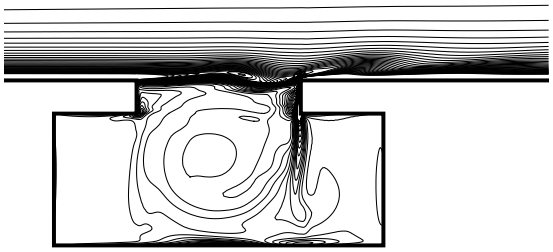

(b) Case P3

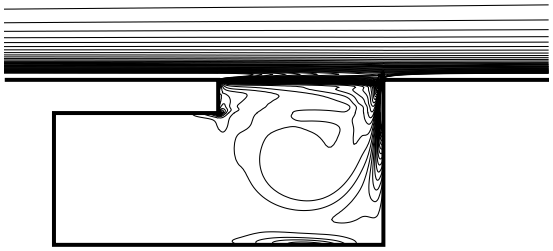

(c) Case P5

Fig.5: Vorticity contours at an instant (50 levels between non-dimensional vorticity, $\omega D/U_\infty = -7$ and 3)

The instantaneous vorticity contours ($\omega = \partial v/\partial x - \partial u/\partial y$) for the cases of different opening positions are shown in figure 5. 50 levels contours are drawn between non-dimensional vorticity ($\omega D/U_\infty$), -7 and 3. The opening length is the same for all cases, but the

strength and frequency of pressure fluctuation are different according to the opening position. The left wall of case P1 and the right wall of case P5 suppress the circulation of the vortex occupying inside the cavity because of the wall boundary effect. The right wall of case P5 suppresses the circulation more than the left wall of case P1, because flow fluctuation of the downstream edge is stronger than that of the leading edge. Therefore the resonance of case P3 is the strongest among these three cases. Case P5 is the weakest and finally becomes the steady mode.

4 ANALYSIS OF MODE TRANSITION

There is a sudden change of Strouhal number between cases H4 and H5 in the assessment of lid thickness variation. In addition, there are sudden changes between cases P2 and P3 and between cases P3 and P4 in the assessment of opening position variation. In this section, the cause of the sudden change of Strouhal number is analyzed through a cross-correlation analysis and the integral form of Rossiter's equation.

The cross-correlation is the time average of the product of two signals with time delay. When one point is fixed and another point is moving in some area, the cross-correlation shows the characteristics of wave propagation in that area. Moreover, the cross-spectral density, which is defined as the Fourier transform of the cross-correlation function, shows a variation of amplitude ratios and phase angles in that area as a function of frequency. The cross-correlation function $R(x_1, x_2, \tau)$ between two points, x1 and x2, is given by the following equation:[15]

$$R(x_1, x_2, \tau) = E[q(x_1, t)q(x_2, t+\tau)] \qquad (2)$$

where q represents the primitive variable (velocity, density, and pressure) and can be expressed as a function of space (x_1 or x_2) and time (t). τ is the time lag between the signals of two points, $q(x_1, t)$ and $q(x_2, t)$. $E[]$ denotes the ensemble averaged value of the quantity in square brackets. The characteristics of wave propagation can be analyzed by Eq. (2).

Rossiter's equation is frequently used as a standard to calculate the frequency of cavity resonance, which is then compared with numerical and experimental results to demonstrate their accuracy. Rossiter's equation is

$$\frac{L}{U_c} + \frac{L}{a_\infty} = \frac{n-\beta}{f_n}, n = 1, 2, 3, \cdots \qquad (3)$$

where L is the cavity length from the leading edge to the downstream edge, U_c is the vortex convection speed, and a_∞ is the free-stream acoustic speed. n is an integer which denotes Rossiter's mode, and f_n is the frequency of the n-th mode. β is the phase lag, which is defined as the phase difference between the vortex and acousic wave at the downstream edge. Eq. (3) can be rewritten as follows.

$$St_n = \frac{f_n L}{U_\infty} = \frac{n-\beta}{M_\infty + 1/k}, n = 1, 2, 3, \cdots \qquad (4)$$

$St_n = f_n L/U_\infty$ is the Strouhal number of the n-th mode, U_∞ is the free-stream velocity, and $M_\infty = U_\infty/a_\infty$ is the Mach number of free-stream. k is a constant defined as the ratio of the vortex convection speed (U_c) to the free-stream velocity (U_∞), $k = U_c/U_\infty$.

The left-hand side of Eq. (3) represents the time needed for one period of cavity resonance mechanism. The first term is the time needed for vortex convection from the leading edge to the downstream edge, and the second term is for acoustic propagation from the downstream edge to the leading edge. It is assumed that the vortex convects downstream at a constant speed U_c, and the acoustic wave propagates upstream at the speed of sound a_∞. β is universally used as 0.25. k varies for each case, because it is determined by fitting Eq. (4) into the experimental results; generally 0.56 is employed.

Although this Rossiter's equation can be easily applied to many cases, it cannot provide exact frequency because it roughly approximates some parameters. Hence, to obtain more precise frequency, the mechanism of cavity resonance is investigated and two parameters, effective length and phase lag, are obtained by intensive study of flow field and wave convection around an open cavity. The integral form of Rossiter's equation[15] is derived by using these parameters and this equation can predict the resonance frequency precisely in various conditions. The integral form of Rossiter's equation is

$$\int_{VG}^{VC} \left(\frac{1}{u} + \frac{1}{a-u}\right) dl_{(\text{along vortex convection path})} = \frac{n-\widetilde{\beta}}{f_n}, n = 1, 2, 3, \cdots \qquad (5)$$

where VG and VC denote the vortex generation point and the vortex collapse point. a and u are local

acoustic speed and vortex convection speed, respectively. The left-hand side is integrated along the path of vortex convection from the vortex generation point to the vortex collapse point. This length, from the vortex generation point to the vortex collapse point, is defined as the effective length. n is an integer which denotes Rossiter's mode, and f_n is the frequency of the n-th mode. Phase lag $\widetilde{\beta}$ is defined as the phase difference of pressure between the vortex collapse point and the acoustic source point. The numerical simulation data are used to calculate this equation.

4.1 Mode Transition of Different Lid Thickness

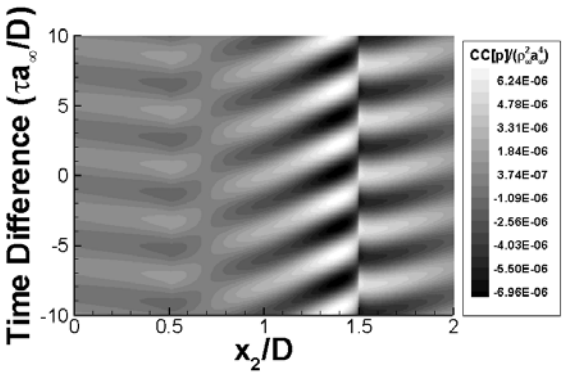

(a) Case H4

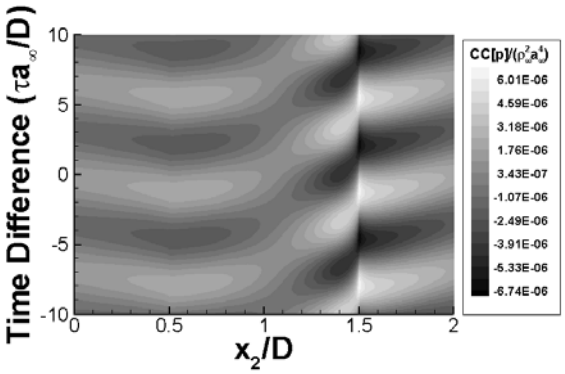

(b) Case H5

Fig.6: Cross-correlation result of pressure when x_1 is fixed at $(x/D, y/D) = (1, 0)$ and x_2 is moving from $(x/D, y/D) = (0, 0)$ to $(x/D, y/D) = (2, 0)$ along x direction. ($CC[p]$: cross-correlation of pressure)

As noted above, there is a sudden change in the Strouhal number between case H4 and case H5 when lid thickness is varied. Cross-correlation analysis (Eq. (2)) and the integral form of Rossiter's equation (Eq. (5)) are used in order to analyze the mode transition and explain the reason of sudden change. Figure 6 shows the results of the cross-correlation for pressure of cases H4 and H5, when x_1 is fixed at $(x/D, y/D) = (1, 0)$ and x_2 is moving from $(x/D, y/D) = (0, 0)$ to $(x/D, y/D) = (2, 0)$ along the x direction. In this coordinate system, the leading edge and the downstream edge of case W0, the rectangular cavity having no lid, are defined at $(x/D, y/D) = (0, 0)$, $(x/D, y/D) = (2, 0)$, respectively. Therefore in case H4 and case H5, the locations of the leading edge and the downstream edge are $(x/D, y/D) = (0.5, 0)$ and $(x/D, y/D) = (1.5, 0)$, because the lid length is $W_1/D = W_2/D = 0.5$. The actual variables of the cross-correlation function are x_2 and τ because x_1 is fixed at a point.

In figure 6, the the results of the cross-correlation for pressure ($CC[p]$) are shown according to the two non-dimensional axes x_2/D and $\tau a_\infty/D$. This shows periodical characteristics in τ direction, because the flow patterns of cases H4 and H5 are the shear layer mode, which has periodical cycle. The period of case H4 is shorter than that of case H5, which constitutes the same result as that the Strouhal number of case H4 is higher than that of case H5 in table 1.

The slope of the ridgeline, as presented in figure 6, represents the direction and speed of wave convection. Gentler slope means faster convection speed, because x-direction of figure 6 is non-dimensional length (x_2/D) and y-direction is non-dimensional time ($\tau a_\infty/D$). When the domain of x_2/D is roughly divided into three regions, $x_2/D < 0.5$, $0.5 < x_2/D < 1.5$, and $1.5 < x_2/D$, the fluctuation of acousic wave is dominant in front ($x_2/D < 0.5$) and behind ($1.5 < x_2/D$) the cavity and that of the flow is dominant near the cavity $0.5 < x_2/D < 1.5$. Thus the convection speeds of each region are $u - a$ ($x_2/D < 0.5$), u ($0.5 < x_2/D < 1.5$), and $u + a$ ($1.5 < x_2/D$). Figure 6 shows a negative velocity in the region of $x_2/D < 0.5$ and the fastest velocity in the region of $1.5 < x_2/D$ because the free-stream Mach number (M_∞) is 0.5.

In the region of the cavity opening ($0.5 < x_2/D < 1.5$), the slope of case H4 is roughly constant from $x_2/D = 0.8$ to $x_2/D = 1.5$. The vortex generated from the leading edge is developed and separated from the shear layer of the leading edge at $x_2/D = 0.8$. This vortex convects downstream with constant speed until collapsing at the downstream edge, $x_2/D = 1.5$. Although the slope of case H5 also changes at $x_2/D = 0.8$, it does not show constant like case H4, because the vortex of case H5 is too weak to separate from

the shear layer of the leading edge. When the slopes of cases H4 and H5 are compared in the region between $x_2/D = 0.8$ and $x_2/D = 1.5$, the slope of case H4 is gentler than that of case H5, which means the vortex convection speed of case H4 is faster than that of case H5. As can be obtained in figure 5, the left and right walls of the opening suppress the rotation of the vortex inside the cavity. As the lid thickness increases, the lid induces more suppression and the convection speed of the vortex in the shear layer decreases. This convection speed of the vortex directly affects the Rossiter's mode, n, in Eq. (3).

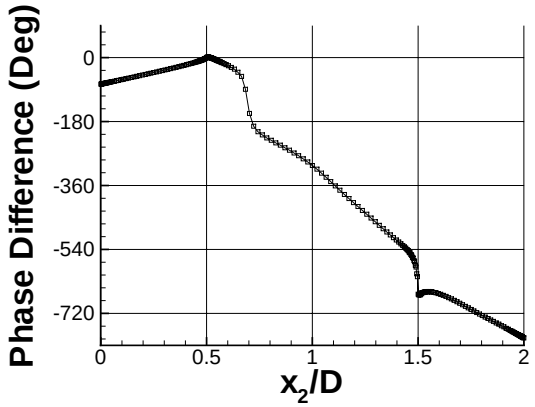

(a) Case H4 ($St = 0.52$)

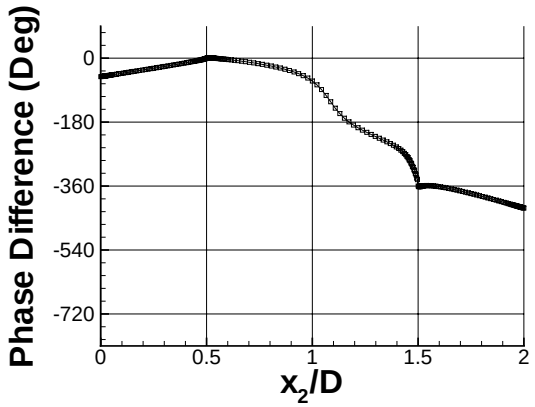

(b) Case H5 ($St = 0.30$)

Fig.7: Phase variation of cross-spectral density for pressure at resonance frequency

The phase of cross-spectral density for pressure is shown in figure 7. The cross-spectral density function is defined as the Fourier transform of the cross-correlation function, as shown in figure 6, and shows an amplitude ratio and phase angle as a function of frequency along the wave propagation. Figures 7(a) and 7(b) show the phase variations of pressure for cases H4 and H5 at the resonance frequency of each case. In table 1, the resonance frequencies of cases H4 and H5 are $St = 0.52$ and $St = 0.30$, respectively. Because this cross-correlation is calculated when x_1 is fixed at $(x/D, y/D) = (1, 0)$, the phase of the cross-spectral density should be zero at $x_2/D = 1$. However, for convenience of interpretation, figure 7 represents the relative phase as that of the leading edge, $(x/D, y/D) = (0.5, 0)$.

In figure 7(a) and 7(b), the phase differences between the leading edge ($x_2/D = 0.5$) and the downstream edge ($x_2/D = 1.5$) are about 720 degrees and 360 degrees, respectively, which means cases H4 and H5 correspond to the second mode ($n = 2$) and first mode ($n = 1$) of Rossiter's equation (Eq. (3)). The concepts of resonance mechanism used in Rossiter's equation imply the total phase change must be a multiple of 360 degrees during one period of cavity resonance loop, in which the vortex in the shear layer convects downstream and the acousic wave generated from the downstream propagate upstream. Figure 7 shows only the phase change of vortex convection from the leading edge to the downstream edge and cannot predict the mode of Rossiter's equation exactly. However, it is possible to roughly predict the mode, because the first term of the left-hand side in Eq. (3), corresponding to the vortex convection term, is much larger than the second term corresponding to the acoustic propagation term.

From the results of cross-correlation and cross-spectral density, it is roughly shown that there is a transition of Rossiter's mode between case H4 and H5. The integral form of Rossiter's equation (Eq. (5)) is analyzed to obtain the exact Rossiter's mode.

The left hand side of Eq. (5) can be calculated by using the numerical simulation data. To determine $\widetilde{\beta}$, which is defined as the phase difference between the vortex collapse point and the acoustic source point, the acoustic source point must be known. Figure 8 shows the root mean square (RMS) contours of pressure around the cavity opening. The point having the maximum value of p_{rms} on wall becomes the dipole acoustic source. Although the maximum value of p_{rms} appears at $(x/D, y/D) = (1.5, -0.04)$ below the downstream edge in case H4, it appears just at the downstream edge in case H5. The pressure signals of the vortex collapse point and the acoustic source point are compared in figure 9. Although the two signals have almost the same phase in case H4, there is a phase lag of 90 degrees in case H5. There is no phase lag when

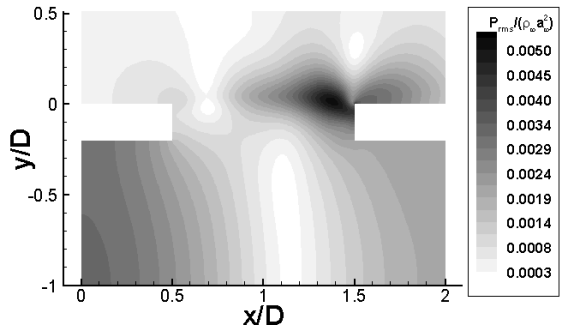

(a) Case H4

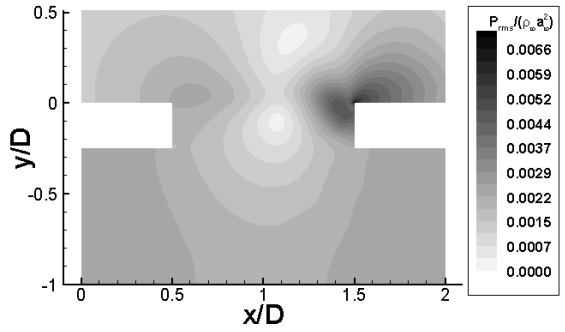

(b) Case H5

Fig.8: RMS (root mean square) contours of pressure around cavity

the acoustic source exists inside the cavity, and there is the phase lag of 90 degrees when acoustic source exists at the downstream edge. This is the same phenomenon as the phase lag of simple rectangular cavity in reference 15. Thus $\widetilde{\beta} = 0$ can be adopted for case H4, and $\widetilde{\beta} = 0.25$ for case H5 because 90 degrees corresponds to 0.25 times of one period.

The results of Eq. (5) are shown in table 2. The predicted Strouhal numbers are compared to the original Rossiter's equation (Eq. (3)) and the exact Strouhal number obtained directly from the far-field acoustic signals of the numerical simulation. In table 2, the predicted Strouhal numbers of Eq. (5) are shown in front of parentheses and those of the original Rossiter's equation (Eq. (3)) are shown in parentheses. In case H4, the predicted Strouhal number of the second mode is 0.53, which shows good agreement with exact Strouhal number, 0.52. In case H5, the predicted Strouhal number of the first mode is 0.29, which also shows good agreement with the value of exact Strouhal number, 0.30.

The results of the cross-correlation analysis and the

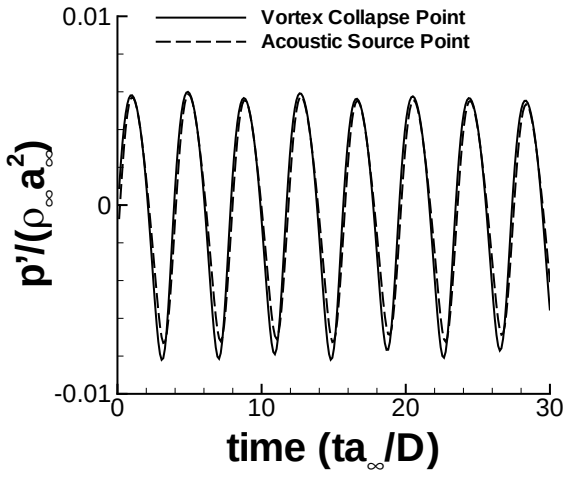

(a) Case H4

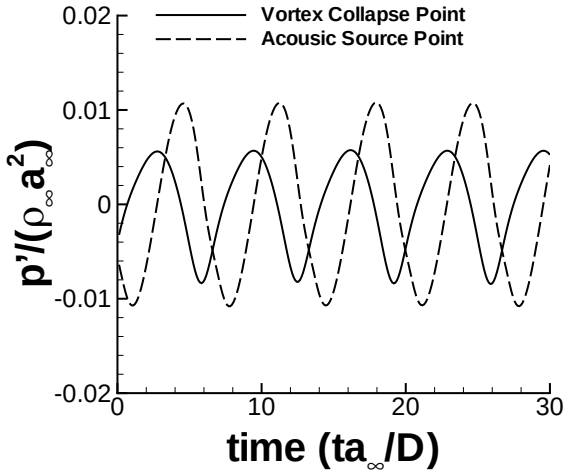

(b) Case H5

Fig.9: Signals of pressure fluctuations at the vortex collapse point and at the acoustic source point

integral form of Rossiter's equation clearly show that case H4 is the second mode of Rossiter's equation, and case H5 is the first mode. Because the left and right walls of the opening suppress the rotation of the vortex inside the cavity, the thick lid induces the convection speed of the vortex in the shear layer to become slow. The slow convection speed then induces the transition of Rossiter's mode from the second mode to the first mode.

Case	$\widetilde{\beta}$	$St(n=1)$	$St(n=2)$	$St(n=3)$	St_{exact}
H4	0	0.27(0.33)	0.53(0.77)	0.80(1.20)	0.52
H5	0.25	0.29(0.33)	0.67(0.77)	1.15(1.20)	0.30
P2	0.25	0.29(0.33)	0.66(0.77)	1.04(1.20)	0.30
P3	0	0.27(0.33)	0.53(0.77)	1.80(1.20)	0.52
P4	0.25	0.30(0.33)	0.71(0.77)	1.11(1.20)	0.30

Table 2. Comparison of the predicted Strouhal number by using integral form of Rossiter's equation (Eq. (5)) and exact Strouhal number (the predicted Strouhal number of the original Rossiter's equation (Eq. (3)) is shown in parenthesis.)

4.2 Mode Transition of Different Opening Position

There are sudden changes of Strouhal number between case P2 and case P3 and between case P3 and case P4 when the opening position is varied. In the same manner as the previous section, cross-correlation analysis (Eq. (2)) and the integral form of Rossiter's equation (Eq. (5)) are used in order to analyze the mode transition and explain the sudden change.

Figure 10 shows the phase variation of cross-spectral density for pressure at the resonance frequency for each case. In table 1, the resonance frequencies of case P2, P3, and H4 are $St = 0.30$, $St = 0.52$ and $St = 0.30$, respectively. In figure 10(a), the phase difference between the leading edge ($x_2/D = 0.25$) and the downstream edge ($x_2/D = 1.25$) is about 360 degrees. And those of figures 10(b) and 10(c) are about 720 degrees and 360 degrees. These results mean that case P2 and case P4 correspond to the first mode ($n = 1$) and case P3 corresponds to the second mode ($n = 2$). As noted above, the left and right walls of the opening suppress the rotation of the vortex inside the cavity. In the case of a central opening, case P3, the suppression of the rotating vortex inside the cavity is the weakest and the convection speed of the vortex in the shear layer is the fastest. Therefore, the Rossiter's mode of case P3 is higher than that of the other cases.

The integral form of Rossiter's equation (Eq. (5)) is analyzed to obtain the exact Rossiter's mode. To determine $\widetilde{\beta}$, figure 11 shows the RMS (root mean square) contours of pressure around the cavity opening. Although the maximum value of p_{rms} appears below the downstream edge in case P3, it appears just at the downstream edge in cases P2 and P4. As the same phenomenon in figure 9, there is no phase lag for case P3, when the acoustic source exists inside the cavity, and there is the phase lag of 90 degrees for cases P2 and P4, when acoustic source exists at the downstream edge. Thus $\widetilde{\beta} = 0.25$ can be adopted for cases P2 and P4, and $\widetilde{\beta} = 0$ for case P3.

The results of Eq. (5) are shown in table 2. In case P3, the predicted Strouhal number of the second mode is 0.53 and shows good agreement with the exact Strouhal number, 0.52. In cases P2 and P4, the predicted Strouhal numbers of the first mode are 0.29 and 0.30, which also show good agreement with the exact Strouhal numbers.

These results clearly show that case P3 is the second mode of Rossiter's equation, and cases P2 and P4 are the first mode. Because the left and right walls of the cavity suppress the rotation of the vortex inside the cavity, the central opening, case P3, induces a higher speed of vortex convection in the shear layer than the other cases. This high convection speed induces the transition of Rossiter's mode from the first mode to the second mode.

5 CONCLUSIONS

The physical phenomena of rectangular open cavities with lids are numerically investigated in this paper. The characteristics of cavity resonance and acoustic propagation are analyzed according to the geometric variation of lids present on the edges of the cavity. The existence of lids changes the resonance frequency, sound pressure level, and directivity of acoustic propagation. The lid induces additional up and down oscillation at the opening and this becomes an acoustic source propagating to the upper direction. As lid length becomes longer, Strouhal number becomes smaller, and steady mode occurs when the lid length is longer than a certain length. As lid thickness becomes thicker, the transition of Rossiter's mode occurs from the second mode to the first mode between case H4 and case H5. For varying opening position, the central open cavity, case P3, shows larger fluctuation than the others, and the backward open cavity, case P5, shows steady mode. There are mode transi-

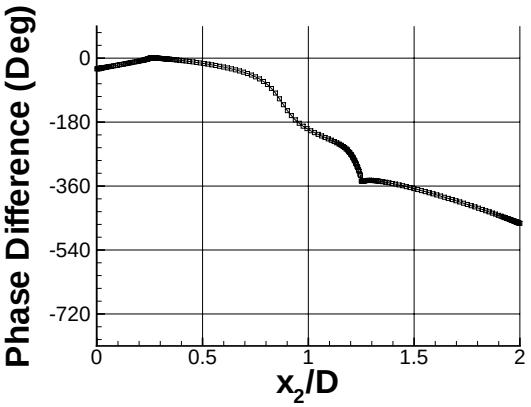

(a) Case P2 ($St = 0.30$)

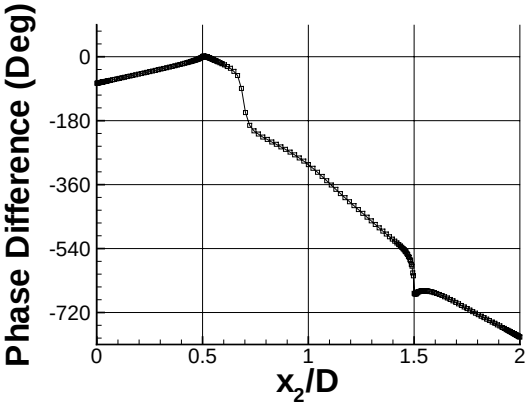

(b) Case P3 ($St = 0.52$)

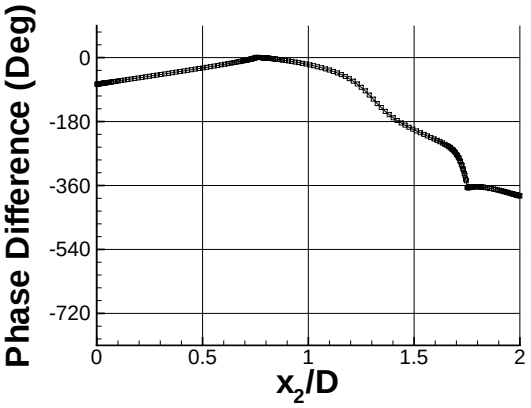

(c) Case P4 ($St = 0.30$)

Fig.10: Phase variation of cross-spectral density for pressure at resonance frequency

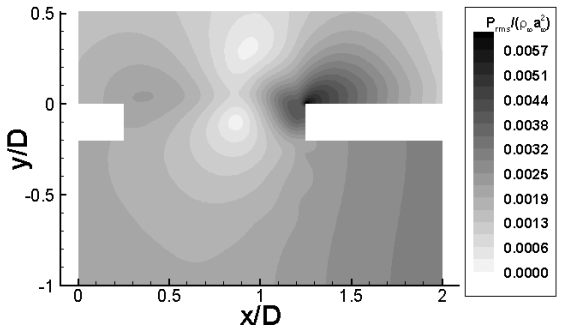

(a) Case P2

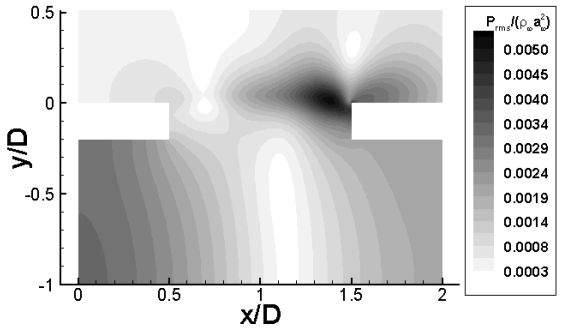

(b) Case P3

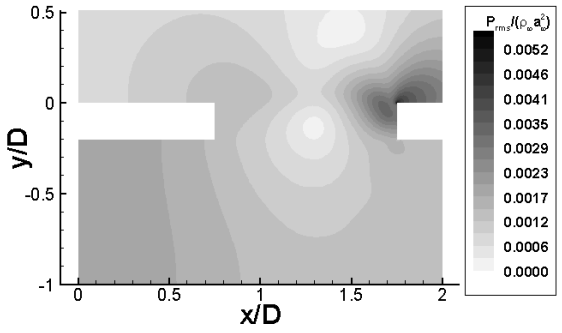

(c) Case P4

Fig.11: RMS (root mean square) contours of pressure around cavity

tions between cases P2 and P3, and between cases P3 and P4. These phenomena can be explained by the wall boundary effect, which suppresses the rotating flow inside the cavity and induce the vortex convection speed in shear layer to become slow. Cross-correlation analysis and the integral form of Rossiter's equation are used to analyze the transition of Rossiter's mode and explain the sudden change of resonance frequency. The result of the cross-correlation analysis shows the wave convection speed and phase variation in space

and time. The left and right walls of the cavity suppress the rotating flow inside the cavity and change the vortex convection speed. The mode transition occurs because of this change in convection speed. The integral form of Rossiter's equation predicts Strouhal number precisely, and shows the mode transition. The present results provide further understanding of cavity resonance and the effects of lid geometry.

Acknowledgement

This research was supported by Basic Research Program of Korea Science and Engineering Foundation under Grant No. R01-1999-000-00264-0.

REFERENCES

[1] Rockwell, D., and Naudascher, E., "Review-Self-sustaining oscillations of flow past cavities," Journal of Fluids Engineering, Transactions of the ASME, Vol. 100, 1978, pp. 152-165.

[2] Krishnamurty, K., "Sound radiation from surface cutouts in high speed flow," PhD thesis, California Institute of Technology, 1956.

[3] Rossiter, J. E., "Wind-tunnel experiments on the flow over rectangular cavities at subsonic and transonic sppeds," Aeronautical Research Council Reports and Memoranda, Technical report 3438, 1964.

[4] Tam, C. K. W., and Block, P. J. W., "On the tones and pressure oscillations induced by flow over rectangular cavities," J. Fluid Mech., Vol. 89, 1978, pp. 373-399.

[5] Cattafesta, L. N. I., Kegerise, M. S., and Jones, G. S., "Experiments on compressible flow-induced cavity oscillations," AIAA paper 98-2912.

[6] Colonius, T., Basu, A. J., and Rowley, C. W., "Numerical investigation of the flow past a cavity," AIAA paper 99-1912.

[7] Rowley, C. W., Colonius, T., and Murray, R. M., "POD based models of self-sustained oscillations in the flow past an open cavity," AIAA paper 2000-1969.

[8] Shieh, C. M., and Morris, P. J., "Comparison of two- and three-dimensional turbulent cavity flows," AIAA paper 2001-0511.

[9] Kim, J. W., and Lee, D. J., "Optimized compact finite difference schemes with maximum resolution," AIAA Journal, vol. 23, No. 5, 1995, pp. 887-893.

[10] Kim, J. W., and Lee, D. J., "Implementation of boundary conditions for optimized high-order compact scheme," Journal of Computational Acoustics, Vol. 5, No. 2, 1997, pp. 177-191.

[11] Hu, F. Q., Hussaini, M. Y., and Manthey, J., "Application of low dissipation and dispersion Runge-Kutta schemes to benchmark problems in computational Aeroacoustics," Procedings of ICASE/LaRC Workshop on Benchmark Problems in computational aeroacoustics, U.S.A., October, 1994.

[12] Kim, J. W., and Lee, D. J., "Adaptive nonlinear artificial dissipation model for computational Aeroacoustics," AIAA Journal, Vol. 39, No. 5, 2001, pp. 810-818.

[13] Kim, J. W., and Lee, D. J., "Generalized characteristic boundary conditions for computational Aeroacoustics," AIAA Journal, Vol. 38, No. 11, 2000, pp. 2040-2049.

[14] Colonius, T., Lele, S. K., and Moin, P., "Boundary conditions for direct computation of aerodynamic sound," AIAA Journal, Vol. 31, 1993, pp. 1574-1582.

[15] Heo, D. N., Kim, J. W., and Lee, D. J., "Study of noise characteristics of an open cavity with cross-correlation analysis," AIAA paper 2003-3104.

[16] Henderson, B., "Category 6 - Automobile noise involving feedback sound generation by low speed cavity flows," Third Computational Aeroacoustics Workshop, Nov., 1999, Cleveland, Ohio.

[17] Gharib, M., and Roshko, A., "The effect of flow oscillations on cavity drag," J. Fluid Mech., Vol. 177, 1987, pp. 501-530.